Journal of Inorganic Biochemistry 176 (2017) 66–76

Contents lists available at ScienceDirect

Journal of Inorganic Biochemistry

journal homepage: www.elsevier.com/locate/jinorgbio

Selective Ru(II)/lawsone complexes inhibiting tumor cell growth by apoptosis

Katia M. Oliveira[a], Luna-Dulcey Liany[b], Rodrigo S. Corrêa[c], Victor M. Deflon[d], Marcia R. Cominetti[b], Alzir A. Batista[a,*]

[a] Departamento de Química, Universidade Federal de São Carlos, CP 676, CEP 13565-905, São Carlos, SP, Brazil
[b] Departamento de Gerontologia, Universidade Federal de São Carlos, CP 676, CEP 13565-905, São Carlos, SP, Brazil
[c] Departamento de Química, Universidade Federal de Ouro Preto, CEP 35400-000 Ouro Preto, MG, Brazil
[d] Instituto de Química de São Carlos, Universidade de São Paulo, CEP 13560-970 São Carlos, SP, Brazil

ARTICLE INFO

Keywords:
Ruthenium complexes
Lawsone
Cytotoxicity
Lung cancer

ABSTRACT

New Ru(II) complexes with lawsone (law) characterized as *trans*-[Ru(law)(PPh_3)$_2$(N-N)]PF_6, where PPh_3 means triphenylphosphine and N-N is 2,2′-bipyridine (**1**), 4,4′-dimethyl-2,2′-bipyridine (**2**), 4,4′-dimethoxy-2,2′-bipyridine (**3**), 1,10-phenanthroline (**4**) or 4,7-diphenyl-1,10-phenanthroline (**5**), induce apoptosis in tumor cells. Cytotoxicity of the complexes against the tumor cell lines DU-145 (prostate cancer cells), MCF-7 (breast cancer cells), A549 (lung cancer cells) and lung non-tumor cell line MRC-5 demonstrated promising IC_{50} values, lower than those found for the cisplatin, a drug used as a reference. Due to the high cytotoxic activity and selectivity against A549 cells line, complex (**5**) was selected for detailed assays. The complex (**5**) inhibits cells migration in concentrations in a nanomolar range, inducing tumor cell death by apoptosis, as confirmed by flow cytometry experiments. Furthermore, the antiproliferative activity of complex (**5**) on A549 tumor cells is attributed to a cell cycle arrest at the Sub G1 phase, followed by a decrease in the number of cells at the S phase. In addition, the interaction of the complexes (**1–5**) with CT-DNA was evaluated by circular dichroism, in which no changes in the secondary structure of DNA were observed, suggesting a weak interaction of the complexes with the biomolecule. On the other hand, complexes (**1–5**) showed a higher interaction with human serum albumin (HSA) by non-covalent van der Waals forces and hydrogen bonding, resulting in static quenching.

1. Introduction

After accidentally discovering cisplatin, the search for metallic compounds endowed with antitumor activities has become a topical area of research in inorganic and coordination chemistry [1,2]. Several four-coordinated platinum(II) analogs have been developed, such as carboplatin and oxaliplatin, however, many of these platinum compounds have showed resistance and high toxicity, increasing side effects, such as nephrotoxicity, neurotoxicity, nausea and vomiting [3–5]. Therefore, the development of new anticancer metallodrugs has focused on complexes with other metals, such as ruthenium, gold, osmium, gallium and others, seeking to obtain compounds with different modes of action [6,7]. The variation of the metal ion provides versatility in terms of designing new drugs, taking into account the variety of oxidation states of the metal center, the coordination number and geometries of the complexes, allowing for adjustments in their chemical reactivity [8,9].

In this context, ruthenium complexes are very promising bioactive agents [10]. So far, the ruthenium complexes, NAMI-A (*trans*-[$RuCl_4$(1*H*-imidazole)(DMSO-S)]), KP1019 (*trans*-[$RuCl_4$(1*H*-indazole)$_2$]), and NKP-1339 (sodium [*trans*-$RuCl_4$(1*H*-indazole)$_2$]) have been evaluated in clinical trials and are effective in treating metastatic tumors [11,12]. Recently, half-sandwich η^6-arene-Ru(II) complexes have been introduced into clinical trials. The complex RAPTA-C ([$RuCl_2$(η^6-p-cymene)(PTA)], PTA = 1,3,5-triaza-7-phosphaadamantane) stands out due to its effective antimetastatic activity in vivo, and low cytotoxicity in vitro [13–15]. This makes these compounds even more attractive, given that the objective of cancer chemotherapy is to eliminate tumor metastasis which is mainly responsible for their ineffectiveness of chemotherapy [9,16].

In metal complexes, the ligands also perform an essential role in the rational design of new drugs because they can increase the biological activity of the compounds, by recognizing specific targets and even changing the chemical reactivity of the complex in the body [8]. Introducing ligands with a previous biological activity can lead to synergistic effects with the metal center or with the complex and is a good

* Corresponding author.
E-mail addresses: kmoliveiraq@gmail.com (K.M. Oliveira), daab@ufscar.br (A.A. Batista).

http://dx.doi.org/10.1016/j.jinorgbio.2017.08.019
Received 3 May 2017; Received in revised form 8 August 2017; Accepted 24 August 2017
Available online 26 August 2017

strategy for metallodrug development. Based on this aspect, a class of natural compounds known as naphthoquinone is associated with many biological activities, such as antibacterial, antifungal, antimalarial and anticancer [17–21]. An example of a naturally occurring compound is known as Lawsone (2-hydroxy-1,4-naphthoquinone), commonly extracted from *Lawsonia alba* [22]. The lawsone can coordinate metals in a bidentate way, O,O^-, forming 5-membered ring [23–25]. In fact, some metal complexes containing lawsone and derivatives as ligands have demonstrated higher biological activity than free lawsone [4,21,26]. Recently, Hartinger and co-workers have reported half-sandwich Ru(II) arene complexes containing lawsone and its derivatives as ligands, which exhibited cytotoxic activity against SW480, CH1/PA-1 and A549 tumor cell lines [4].

As part of our ongoing effort to design new metallodrug candidates with antitumor activity, in recent years our research group has reported some ruthenium complexes containing phosphines and diimines as ligands with promising results against this disease [27–30]. Therefore, in this paper we have synthesized and characterized five new ruthenium complexes containing phosphines, diimines and lawsone as ligands. The cytotoxicity assays, in vitro, of the ruthenium complexes against human tumor cell lines, including breast, prostate and lung and against one lung non-tumor human cell line, were carried out using the MTT method. In addition, we analyzed the effect of ruthenium complexes on cell morphology and migration, as well as the mechanism of cell death induced and changes in cell cycle arrest by flow cytometry. Furthermore, their ability to interact with CT-DNA and HSA were investigated.

2. Experimental

2.1. Material and methods

All chemicals used to prepare the complexes and buffer solution are of analytical grade or chemically pure grade. All the synthesis of the complexes was carried under argon atmosphere. The $RuCl_3{\cdot}3H_2O$, triphenylphosphine (PPh_3), N-N = 2,2′-bipyridine (bipy), 4,4′-dimethyl-2,2′-bipyridine (mebipy), 4,4′-dimethoxy-2,2′-bipyridine (meobipy), 1,10-phenanthroline (phen), 4,7-diphenyl-1,10-phenanthroline (phphen) and lawsone (law) were used as received from Aldrich. KPF_6, salts used for buffer preparation, CT-DNA (Calf Thymus), HSA (Human Serum Albumin) and MTT (3-(4,5-dimethylthiazol-2-yl)-2,5-diphenyltetrazolium bromide) were purchased from Aldrich.

2.2. Physical measurements

The NMR experiments ($^{31}P\{^1H\}$,$^{13}C\{^1H\}$, ^1H) were recorded on a 9.4 T Bruker Avance III spectrometer in DMSO-d_6. The $^{31}P\{^1H\}$ shifts are reported in relation to H_3PO_4 85%. The experiments of ^1H-^1H gCOSY, ^1H-^{13}C gHSQC, and ^1H-^{13}C gHMBC were carried out for complete characterization of ruthenium complexes. Elemental analyses (C, H and N) were performed on a Fisons EA 1108 model (Thermo Scientific) equipment. UV–Visible (UV–vis) was recorded on a Hewlett Packard diode array – 8452A spectrophotometer. IR spectra between 4000 and 200 cm^{-1} were registered using as CsI pellets on a Bomem-Michelson FT-MB-102 instrument. Fluorescence spectra were performed by using a fluorimeter Synergy/H1-Biotek. The circular dichroism spectra were obtained from a spectropolarimeter Jasco J-720, using the quartz cuvette circular of 1 cm path length. The electrochemical experiments were carried using a BAS, model 100B at room temperature in CH_2Cl_2 containing 0.10 M tetrabutylammonium perchlorate (TBAP) (Fluka Purum) as a support electrolyte. The working and auxiliary electrodes were stationary Pt foils, and the reference electrode was Ag/AgCl, 0.10 M TBAP in CH_2Cl_2, in a Luggin capillary probe. Conductivity values were obtained using a MeterLab CDM2300 at room temperature.

2.3. Synthesis and characterization

2.3.1. Synthesis of cis,trans-[$RuCl_2(PPh_3)_2$(N-N)], general procedure

The synthesis of the complex precursors was carried out following procedures described by Batista and coworkers [31]. For this, the N-N ligand (0.25 mmol) was added to the solution of [$RuCl_2(PPh_3)_3$] (0.20 mmol, 0.2 g) in 20 mL of CH_2Cl_2. The reaction was kept in agitation under argon atmosphere for 1 h. After that, the solution volume was reduced to approximately 2 mL and ethyl ether was added to precipitate a brown solid. The solid was filtered, washed with ethyl ether and dried under vacuum.

2.3.2. Synthesis of trans-[Ru(law)$(PPh_3)_2$(N-N)]PF_6, general procedure

To obtain the new complexes (**1–5**), the lawsone (0.18 mmol; 0.031 g) was dissolved in 50 mL of a mixture of CH_2Cl_2:CH_3OH (1:1 v/v) in a Schlenk flask, containing 80 μL of triethylamine. Then, (0.12 mmol) of *cis,trans*-[$RuCl_2(PPh_3)_2$(N-N)] and (0.24 mmol; 0.044 g) KPF_6 was added. The solution was kept under reflux, inert atmosphere and was stirred for 12 h. The solution with a dark color was concentrated to ca. 5 mL, and water was added to precipitate a powder. The solids were filtered off, washed with water and diethyl ether (3 × 15 mL each) and dried under vacuum.

trans-[Ru(law)$(PPh_3)_2$(bipy)]PF_6 (**1**): Yield: 49.66 mg (77%). Anal. Calc. for [$C_{56}H_{43}F_6N_2O_3P_3Ru$]·1/2 CH_2Cl_2: exp. (calc) C, 60.92 (61.15); H, 4.02 (3.94); N, 2.52 (2.55) %. Molar conductivity in CH_2Cl_2, 33.96 S cm^2 mol^{-1}. IR (Selected bands, cm^{-1}): ν(C_1=O) 1602, ν(C_4=O) 1618, ν(C_2–O) 1091. $^{31}P\{^1H\}$ NMR δ(ppm): 30.68 (s). ^1H NMR (400 MHz, DMSO-d_6, 298 K): δ(ppm): 5.53 (s, 1H, law), 9.86 (m, 1H, bipy), 9.37 (m, 1H, bipy), 8.14–6.97 (overlapped signals, 30H aromatic hydrogen for PPh_3, 6H for bipy and 4H for law). ^{13}C NMR (400 MHz, DMSO-d_6, 298 K): δ(ppm) 198.55 (C_1=O of law), 181.52 (C_4=O of law), 170.46 (C_2–O of law).

trans-[Ru(law)$(PPh_3)_2$(mebipy)]PF_6 (**2**): Yield: 48.02 mg (75%). Anal. Calc. for [$C_{58}H_{47}F_6N_2O_3P_3Ru$] exp. (calc) C, 61.95 (61.76); H, 4.78 (4.20); N, 2.33 (2.48) %. Molar conductivity in CH_2Cl_2, 40.20 S cm^2 mol^{-1}. IR (Selected bands, cm^{-1}): ν(C_1=O) 1600, ν(C_4=O) 1610, ν(C_2–O) 1093. $^{31}P\{^1H\}$ NMR δ(ppm): 30.06 (s). ^1H NMR (400 MHz, DMSO-d_6, 298 K): δ(ppm): 2.30 (s, 3H, CH_3 of mebipy), 2.41 (s, 3H, CH_3 of mebipy), 5.59 (s, 1H, law), 9.65 (m, 1H, bipy), 9.23 (m, 1H, bipy), 8.16–6.98 (overlapped signals, 30H aromatic hydrogen for PPh_3, 4H for mebipy and 4H for law). ^{13}C NMR (400 MHz, DMSO-d_6, 298 K): δ(ppm): 198.53 (C_1=O of law), 181.46 (C_4=O of law), 170.63 (C_2–O of law).

trans-[Ru(law)$(PPh_3)_2$(meobipy)]PF_6 (**3**): Yield: 50.83 mg (80%). Anal. Calc. for [$C_{58}H_{47}F_6N_2O_5P_3Ru$] exp. (calc) C, 60.31 (60.05); H, 4.18 (4.08); N, 2.12 (2.41) %. Molar conductivity in CH_2Cl_2, 31.60 S cm^2 mol^{-1}. IR (Selected bands, cm^{-1}): ν(C_1=O) 1599, ν(C_4=O) 1614, ν(C_2–O) 1092. $^{31}P\{^1H\}$ NMR δ(ppm): 31.46 (s). ^1H NMR (400 MHz, DMSO-d_6, 298 K): δ(ppm): 3.85 (s, 3H, CH_3 of meobipy), 3.91 (s, 3H, CH_3 of meobipy), 5.47 (s, 1H, law), 9.51 (m, 1H, meobipy), 9.05 (m, 1H, meobipy), 8.12–7.00 (overlapped signals, 30H aromatic hydrogen for PPh_3, 4H for meobipy and 4H for law). ^{13}C NMR (400 MHz, DMSO-d_6, 298 K): δ(ppm): 198.59 (C_1=O of law), 181. 30 (C_4=O of law), 170.75 (C_2–O of law).

trans-[Ru(law)$(PPh_3)_2$(phen)]PF_6 (**4**): Yield: 46.14 mg (73%). Anal. Calc. for [$C_{58}H_{43}F_6N_2O_3P_3Ru$]·1/2 CH_2Cl_2 exp. (calc) C, 62.03 (61.98); H, 3.95 (3.86); N, 2.33 (2.49) %. Molar conductivity in CH_2Cl_2, 39.30 S cm^2 mol^{-1}. IR (Selected bands, cm^{-1}): ν(C_1=O) 1599, ν(C_4=O) 1616, ν(C_2–O) 1096. $^{31}P\{^1H\}$ NMR δ(ppm): 30.08 (s). ^1H NMR (400 MHz, DMSO-d_6, 298 K): δ(ppm): 5.59 (s, 1H, law), 10.24 (m, 1H, phen), 9.70 (m, 1H, phen), 8.47–6.82 (overlapped signals, 30H aromatic hydrogen for PPh_3, 6H for phen and 4H for law). ^{13}C NMR (400 MHz, DMSO-d_6, 298 K): δ(ppm): 198.83 (C_1=O of law), 181.54 (C_4=O of law), 170.68 (C_2–O of law).

trans-[Ru$(PPh_3)_2$(law)(phphen)]PF_6 (**5**): Yield: 37.80 mg (70%). Anal. Calc. For [$C_{70}H_{51}F_6N_2O_3P_3Ru$] exp. (calc) C, 65.36 (65.88); H,

4.28 (4.03); N, 2.16 (2.20)%. Molar conductivity in CH_2Cl_2, 36.07 Ω^{-1} cm^2 mol^{-1}. IR (Selected bands, cm^{-1}): ν(C_1=O) 1598, ν (C_4=O) 1613, ν(C_2–O) 1091. $^{31}P\{^1H\}$ NMR δ(ppm): 29.85 (s). ^1H NMR (400 MHz, DMSO-d_6, 298 K): δ(ppm): 5.65 (s, 1H, law), 10.35 (m, 1H, phphen), 9.82 (m, 1H, phphen), 8.27–6.94 (overlapped signals, 30H aromatic hydrogen for PPh_3, 14H for phphen and 4H for law). ^{13}C NMR (400 MHz, DMSO-d_6, 298 K): δ(ppm): 198.73 (C_1=O of law), 181.61 (C_4=O of law), 170.71 (C_2–O of law).

2.4. Crystal structure determination

Crystals of complexes (**2**) and (**5**) were obtained at room temperature from dichloromethane/ether (1:1) solution, and were mounted on glass fibers. A Bruker Kappa APEX II Duo diffractometer, equipped with graphite monochromated MoKα radiation (λ = 0.71073 Å), was used for intensity data collection at room temperature. The structure of complexes (**2**) and (**5**) was solved with SHELXS and refined with SHELXL software [32], with anisotropic thermal displacements for all non-hydrogen atoms. More information about the crystal structure and refinement data is depicted in Table S1. Supplementary crystallographic data are deposited with the number 1545005 and 1545006 for complexes (**2**) and (**5**), respectively, being obtained free of charge from The Cambridge Crystallographic Data Centre via www.ccdc.cam.ac.uk/structures.

2.5. DNA binding study by circular dichroism (CD)

Solutions of CT-DNA were prepared by diluting about 40 mg of CT-DNA in 20 mL of Tris-HCl buffer (5 mM Tris-HCl and 50 mM NaCl, pH 7.4). The concentration of CT-DNA was determined using the molar extinction coefficient of 6600 M^{-1} cm^{-1} at 260 nm. The CD spectra were recorded in the presence of constant concentration of the CT-DNA, with increasing of the ruthenium complex concentrations. The measures were collected from 240–350 nm at 298 K and under constant nitrogen flush. The stock solutions of ruthenium complexes were prepared in DMSO at a concentration of 1.5 mM. The molar ratios used (Ri = [complexes] / [CT-DNA]) were: 0.05 to 0.4. The samples were incubated at 310 K for 18 h.

2.6. Protein binding studies

HSA solution was prepared by dissolving the protein in a Tris-HCl buffer. The exact concentration of HSA (5 μM) was determined by absorption spectrophotometric analysis, using the molar extinction coefficient of 35,700 M^{-1} cm^{-1} at 280 nm [33]. The experiment was performed using an opaque 96-well plate. The excitation wavelength was set at 270 nm and the emission was read at 300–600 nm. Stock solutions of ruthenium complexes were prepared in DMSO and incubated with HSA protein in different molar ratios of complexes/HSA. Measurements were recorded at temperatures of 298 and 310 K.

2.7. Biological evaluation

2.7.1. Cell viability assay

The cytotoxic activity of ruthenium complexes was evaluated against different human carcinoma cells: DU-145 (prostate; ATCC: HTB-81), MCF-7 (breast; ATCC: HTB-22), A549 (lung; ATCC: CCL-185) and MRC-5 (lung; ATCC: CCL-171) non-tumorigenic cell line, using the MTT colorimetric assay. The cells were cultured in Dulbecco's Modified Eagle's Medium (DMEM) for A549 and MRC-5, supplemented with 10% fetal bovine serum (FBS) or Roswell Park Memorial Institute (RPMI) 1640 Medium for DU-145 and MCF-7, supplemented with 20% FBS, at 310 K in humidified 5% CO_2 atmosphere. To conduct the assay, 1.5×10^4 cells/well were seeded in 200 μL of medium in 96-well plates (Corning Costar). The cells were maintained for 24 h to attach and then were treated with ruthenium complexes for 48 h. The ruthenium complexes were dissolved in DMSO, and 1 μL was added to wells with 200 μL of medium, resulting in the concentration ranges (50–0.003 μM). Cisplatin, used as a reference drug, was solubilized in DMF. After the treatment, MTT (30 μL, 1 mg mL^{-1} in PBS) was added to each well, and the plate was incubated for 3 h. Cell viability was detected by reducing MTT to purple formazan in living cells. The formazan crystals were solubilized by isopropanol (100 μL/well), and the optical density of each well was measured using a microplate spectrophotometer at a wavelength of 540 nm. The Inhibitory Concentration to 50% (IC_{50}) of cell proliferation (Table 3) was obtained from the analysis of absorbance data of three independent experiments.

2.7.2. Cell morphology

The morphology of A549 and MRC-5 cells was analyzed in the presence of different concentrations of complex (**5**) (0.01–10 μM). Therefore, 1×10^5 cells/well were seeded in 1 mL of medium in 12-well plates (Corning Costar) and maintained to attach at 24 h 310 K in 5% CO_2. Cells were treated with complex (**5**) and images of cell morphology were recorded at 0, 24 and 48 h of incubation using an inverted microscope (Nikon Eclipe TS100) coupled to a still camera (Moticam 1000–1.3MP Live Resolution) with an amplification of 40 ×.

2.7.3. Wound healing

For this assay, A549 cells were seeded at a density of 1×10^5 cells/well in 12-well plates and maintained to attach at 310 K in 5% CO_2 for 24 h, until reaching confluency. A wound was created in the confluent monolayer using pipette tips. The culture medium containing cells in suspension was removed. A new culture medium was added containing different concentrations of complex (**5**). Images of each wound were recorded using an inverted microscope (Nikon Eclipe TS100) coupled to a camera (Moticam 1000 – 1.3 MP Live Resolution) with an amplification of 10 ×, at different times (0–48 h). The wound closure was analyzed by the recorded images using Image J software.

2.7.4. Cell migration study

A Transwell migration assay was conducted using a 24-well chamber (BD Biosciences, Franklin Lakes, NJ, USA). For this assay, A549 cells (0.5×10^5 cell/well) were suspended in DMEM serum-free and added in the upper chamber, together with different concentrations of complex (**5**). In the lower wells, DMEM was added with 10% FBS and plates were incubated at 310 K and 5% CO_2 for 22 h. Non-migrating cells that remained on the upper membrane surface were removed using cotton swabs. The cells that migrated to the lower membrane surface were fixed with methanol for 10 min, stained with toluidine blue and washed with distilled water. Images were acquired using an inverted microscope (Nikon Eclipe TS100) coupled to a camera (Moticam 1000–1.3MP Live Resolution) with amplification of 40 ×. The cells were counted using Image J software.

2.7.5. Cell cycle analysis

A549 cells were seeded in 12-well plates at a density of 1.5×10^5 cells/well. After 24 h, different concentrations (1, 2 and 3 μM) of complex (**5**) were added to the wells for 24 h. For control, only DMSO was added to the cells. After that, cells were collected, centrifuged (5 min at 1200 rpm), harvested in cold PBS and fixed with 70% aqueous ethanol (v/v). The cells were stored at − 20 °C overnight. Posteriorly, the cells were centrifuged (5 min at 1500 rpm), resuspended in 300 μL of RNase A (0.2 mg mL^{-1}) and incubated for 30 min at 37 °C. Then, the samples were stained for 1 h with hypothonic fluorochrome solution (Propidium iodide 5 μg mL^{-1} sodium citrate 0.1% and Triton-X-100 0.1%). After that, the samples were analyzed by flow cytometry (Accuri C6 BD Biosciences). The number of cells analyzed for the sample was 10,000 and the assay was performed in triplicate.

2.7.6. Apoptosis assay

Cell death was evaluated using the Annexin V-PE apoptosis

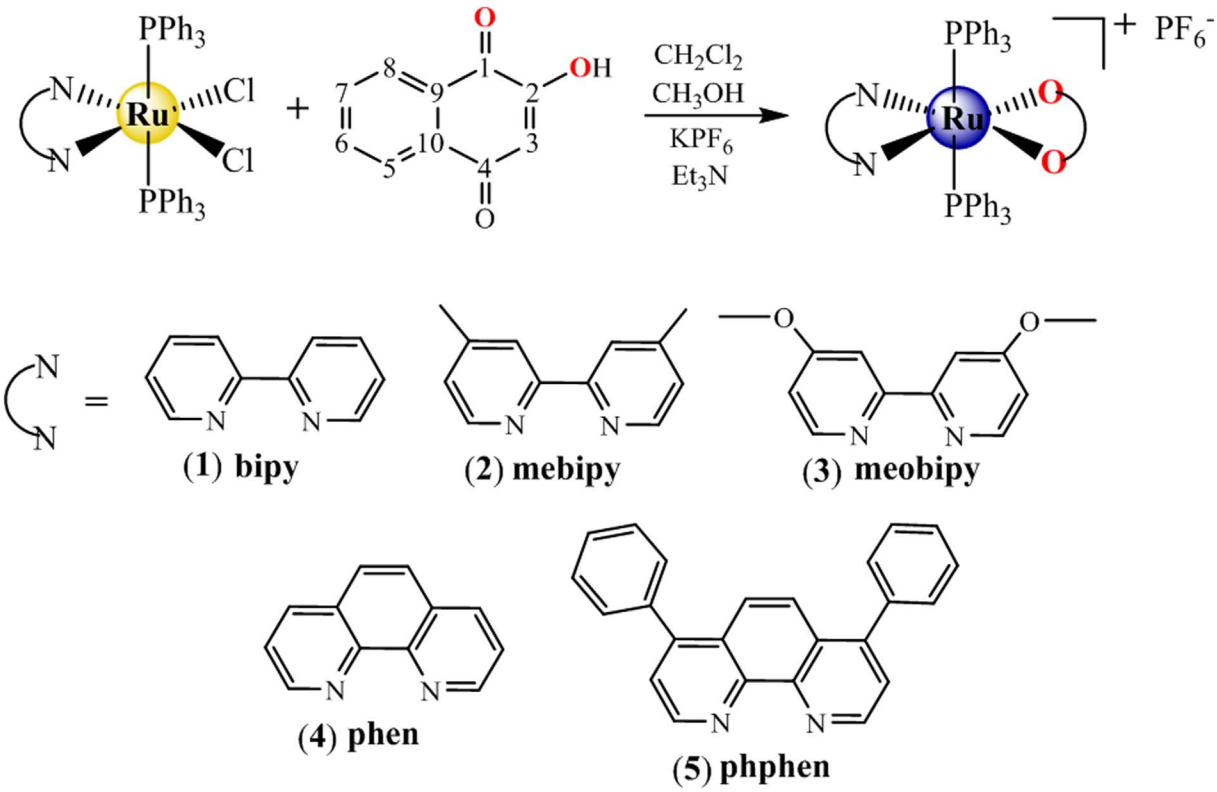

Scheme 1. The synthetic route of ruthenium complexes (**1–5**).

detection kit (BD Biosciences) according to the instruction manual. A549 cells (0.8×10^5 cells/well) were seeded on 24-well plates (Corning Costar) and maintained to attach at 37 °C in 5% CO_2 for 24 h. On the next day, different concentrations (3, 10 and 20 μM) of the complex (**5**) were added to the wells and incubated for 24 h. After treatment, the plate was centrifuged at 2000 rpm for 5 min and 4 °C, the medium was collected and cells were washed in ice-cold PBS. Next, the binding buffer (200 μL), 2.5 μL of 7-AAD and 2.5 μL of PE were mixed to the cells, which were incubated for 20 min in the dark. Then, the plate was centrifuged at 2000 rpm for 5 min and 4 °C and 200 μL of binding buffer were added. The cells were removed and transferred to tubes and then analyzed using a flow cytometer BD Accuri C6 Plus.

3. Results and discussion

3.1. Synthesis and characterization

Dark blue or purple ruthenium complexes (**1–5**) containing lawsone were obtained according to the procedure illustrated in Scheme 1. The synthetic route obtained pure complexes with good yields (~80%) according to spectroscopic data, as well as elemental analyses, molar conductivity and $^{31}P\{^1H\}$, ^1H and ^{13}C NMR spectrum. All complexes are air-stable solids. The stability of the complexes, in solution, was evaluated by $^{31}P\{^1H\}$ NMR spectroscopy in DMSO, and they are stable for at least 72 h (Fig. S1 Supplementary information).

The molar conductivity measurements for the ruthenium complexes (**1–5**), in dichloromethane, present values that are consistent with a 1:1 electrolyte (31.60–40.20 S cm^2mol^{-1}), which agree with complexes with a general formula $[Ru(L)(PPh_3)_2(bipy)]PF_6$ previously reported [28].

The solid-state FT-IR experiments were carried out for free lawsone and for complexes (**1–5**). Based on these spectra, some important band displacements were observed, which was useful for the preliminary confirmation of the ligand coordination of the binder to the metal center. The spectrum of the free lawsone displays a broad band around 3175 cm^{-1} assigned to ν(O—H) stretching vibrations. In the spectra of complexes (**1–5**), this band is absent, indicating deprotonation and coordination of the hydroxyl oxygen atom [25]. In the region of 1800 to 1700 cm^{-1} displacement of the $\nu(C_1{=}O)$ stretching vibration was observed, which changed from 1640 to 1602 cm^{-1}, due to the weakening of the double bond after coordination to the ruthenium. The band related to $\nu(C_4{=}O)$ also presented a small displacement, from 1679 to 1618 cm^{-1}. In addition, the $\nu(C_2{-}O)$ stretching of the free ligand lawsone (observed at 982 cm^{-1}) underwent a higher wavenumber upon complexation. This was observed at 1091 cm^{-1} [34]. This behavior was also observed for other complexes containing the lawsone as ligand [25,35–37]. Additionally, the absorptions at 841 and 558 cm^{-1} are assigned to the counter-ion PF_6^{-1}. The bands in 514 and 400 cm^{-1} can be attributed to ν(Ru–O) and ν(Ru–N), respectively [38].

Electronic spectra of the ruthenium complexes (**1–5**) showed three absorptions around 268, 290 and 580 nm (see Supporting information, Fig. S7). The absorptions at 268 and 290 nm are assigned $\pi \rightarrow \pi^*$ transitions of phosphines, diimine derivatives and lawsone ligands. Meanwhile, the absorption at around 580 nm can be assigned to $n \rightarrow \pi^*$ transitions, which is characteristic of quinones coordinated to metals [39,40]. This band can also be attributed to metal-to-ligand charge transfer (MLCT) transitions from Ru(dπ) to the ligand (π*).

The electrochemical studies of the ruthenium complexes (**1–5**), carried out using the cyclic voltammetry technique, were performed in CH_2Cl_2 solutions containing 0.10 M TBAP. The complexes (**1–5**) exhibit Ru(II)/Ru(III) irreversible oxidation processes at about 1000 mV, which are higher than those values found for the respective precursor complexes (range 300–400 mV) [31], indicating more stability of the metal center after coordination of the lawsone ligand. This metal center stabilization is possible due to the replacement of two σ and π donor chlorides by a monocharged chelating lawsone ligand.

The analysis of the $^{31}P\{^1H\}$ NMR of complexes (**1–5**) showed one singlet around 30 ppm, due to the equivalence of the two PPh_3 ligands in *trans* configuration. These values are similar for compounds such as the *trans*-$[Ru(PPh_3)_2(N\text{-}N')(bipy)]PF_6$, N-N′ = *N*-(acyl)-*N*′,*N*′-(di-

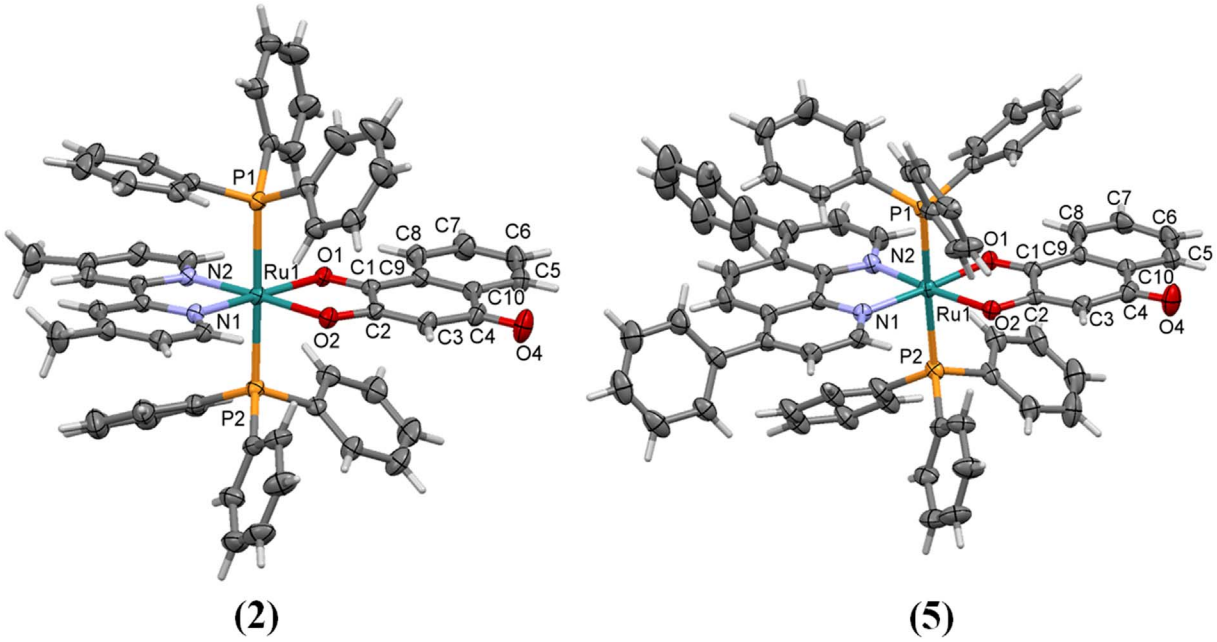

Fig. 1. Crystal structures of complexes (**2**) and (**5**) showing the atom numbering scheme and displacement ellipsoids (30% probability level).

substituted)thioureas [28], and common for ruthenium complexes containing two PPh_3 in *trans* position to each other [21,27]. The complexes containing lawsone as ligand showed higher chemical shifts compared to the precursors, in which the singlet signals occur at around 22 ppm [41].

The ^1H NMR spectra for complexes (**1–5**) show that the absence of the hydroxyl hydrogen signal is in accordance with the deprotonation of the OH upon coordination. For all the complexes, overlapping of the signals were observed. For complex (**5**) in the region of 8.27–6.94, ppm multiplets were observed corresponding to 48 aromatic hydrogen atoms from the phosphines, diimines and lawsone. In the 5.65 ppm, the singlet of the hydrogen atom bonded to carbon 3 can be observed. In addition, multiplet signals occurring at 10.35 and 9.82 ppm are assigned to the phphen ligand (see Supporting information, Figs. S2–S6).

Single crystals suitable for X-ray diffraction were obtained for complexes (**2**) and (**5**). Fig. 1 shows the stereochemistry and coordination sphere around the metal center by the MERCURY representation. The crystallographic data are given in Supplementary Material. The complex (**2**) crystallized in the monoclinic system with space group C 2/c, and complex (**5**) in triclinic P-1 one with two molecules in the asymmetric unit. Both complexes present a distorted octahedral geometry, as observed by the bond angles (Table 1). These values agree very well with those values obtained for complexes containing PPh_3 as ligands [21], [30,42]. The values obtained for N-Ru-N and O-Ru-O bond angles on the equatorial position are distant of the 90°, indicating the tension of the five-membered chelate ring of the diimines and lawsone. The bond angles for P-Ru-N and P-Ru-P are close to 90° and 180°, respectively. As can be seen the Ru(II) ion is coordinated to lawsone anion acting as bidentate ligand through their carbonyl and deprotonated phenolic oxygen atoms (Ru-O1 and Ru-O2 distances are 2.0946(18) and 2.1032(18) Å, for complex (**2**) and 2.064(2) and 2.127(2) Å for complex (**5**), respectively).

Comparing the O−C bond lengths values of lawsone free of metal [43] with those ones obtained to metal complexes studied here, the O(1)−C(1) bond lengths to complexes (**2**) and (**5**) [1.249(3) and 1.250(4) Å, respectively] are larger than O(1)−C(1) bond length one of lawsone free [1.212 Å], as a result of ligand coordination. On the other hand, the O(2)−C(2) bond length in the free ligand is 1.334 Å, while the complexes (**2**) and (**5**) present values of 1.294(3) and 1.294(4) Å, respectively, suggesting a double bond character enhancement due to resonance in the O1−C1−C2−O2 moiety of the ligand. Such resonance also affect the C(1)-C(2) bond with value of 1.505 Å in lawsone free (single bond character), while in the metal complexes this bond is slightly shortened (Table 1).

Table 1
Selected bond distances (Å) and angles (°) for complexes (**2**) and (**5**).

Fragment	(2)	(5)
Ru(1)-O(1)	2.0946(18)	2.064(2)
Ru(1)-O(2)	2.1032(18)	2.127(2)
Ru(1)-P(1)	2.4149(8)	2.3841(9)
Ru(1)-P(2)	2.3934(8)	2.4049(10)
Ru(1)-N(1)	2.041(2)	2.060(3)
Ru(1)-N(2)	2.040(2)	2.023(3)
O(1)-C(1)	1.249(3)	1.250(4)
O(2)-C(2)	1.294(3)	1.294(4)
O(4)-C(4)	1.228(4)	1.244(5)
C(1)-C(2)	1.482(4)	1.486(5)
O(1)-Ru(1)-O(2)	76.40(7)	76.93(9)
O(1)-Ru(1)-P(1)	90.63(5)	90.18(7)
O(2)-Ru(1)-P(2)	88.15(6)	87.65(7)
O(1)-Ru(1)-P(2)	89.57(5)	90.21(7)
P(2)-Ru(1)-P(1)	178.61(3)	176.75(4)
N(2)-Ru(1)-N(1)	78.07(9)	78.73(12)
N(1)-Ru(1)-P(2)	91.09(6)	90.23(8)

3.2. DNA binding studies

DNA macromolecule is a biological target to be studied considering the design of new compounds to act in anticancer chemotherapy, given that the process of cell division involves DNA replication [44]. To explore the complex/DNA interaction ability, the Circular Dichroism (CD) technique was used in order to evaluate the DNA conformation changes caused by the ruthenium complexes. This technique presents high sensitivity to identify alterations on the DNA secondary structure [44]. A typical spectrum of CT-DNA exhibits two bands in the UV region, a positive band at 275 nm due to base stacking and a negative band at 245 nm due to right-handed helicity [45,46]. CT-DNA bands were monitored by adding different molar ratios of the complexes and CT-DNA (Ri = [Complex] / [CT-DNA] = 0.05 to 0.4). The CT-DNA spectra, both free and in the presence of complex (**5**), can be seen in

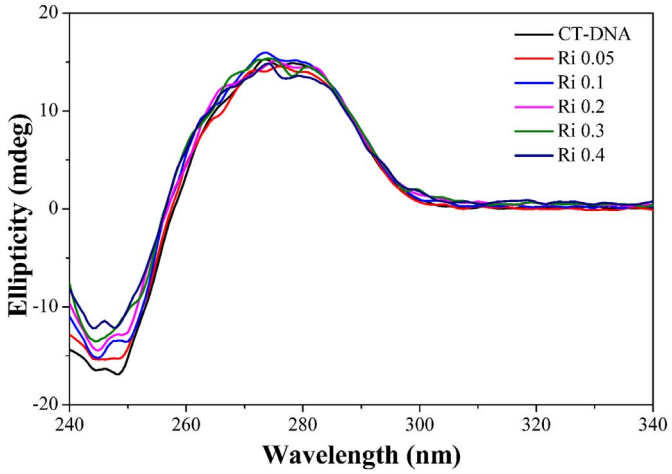

Fig. 2. CD spectra of CT-DNA (50 μM) incubated with complex (**5**) for 18 h at 310 K in different molar ratios.

Fig. 2.

In general, compounds that exhibit electrostatic interaction with DNA show no significant changes in CT-DNA bands, while compounds that exhibit covalent interactions or intercalation cause changes in their secondary structure. When adding complex (**5**) (Fig. 2), it can be observed that there were no significant changes in the secondary CT-DNA structure, under our experimental conditions. This result indicates that the complex (**5**) has a weak interaction with the CT-DNA, which can be electrostatic interaction due to the positive charge of the complex. The same behavior was observed for all synthesized complexes here (see Supporting information, Fig. S8). The weak interaction of our complexes with DNA suggests that this biomolecule cannot be the primordial target for their activity, as observed for other ruthenium complexes reported in the literature [47,48]. Thus, the antitumor activity may be related to other biological targets, such as topoisomerases and kinases.

3.3. Protein binding studies

HSA is the most abundant protein of the circulatory system and carries out various important functions, such as transporting drugs and nutrients through the organism [28]. Therefore, it is important to know the type of drug/HSA interaction to better understand the drug's biochemical and physiological effects. The HSA displays fluorescence mainly due to the presence of a tryptophan residue located in subdomain II, at position 214 [49]. Changes in the conformation of HSA due to the presence of ruthenium complexes can affect their fluorescence and indicate interactions with protein. Thus, we have decided to investigate the behavior of ruthenium complexes in the presence of HSA, evaluating their temperature dependence. The fluorescence spectra of HSA in the absence and presence of ruthenium complexes (**1–5**) was obtained in 298 and 310 K, with excitation at 270 nm. Concentrations of complexes were in the range of 0 to 25 μM and the HSA concentration was fixed at 5 μM.

The fluorescence intensity of quenched HSA decreased significantly when increasing concentrations of the complexes were added, as can be observed in Fig. 3. Fluorescence suppression of HSA can occur by two types of mechanisms: dynamic and static. Dynamic quenching occurs when the fluorophore comes in contact with the quencher (ruthenium complexes) during the transient existence of the exited state, while the static mechanism occurs with the formation of the HSA/complex species in the ground state of the fluorophore-quencher [50]. These two mechanisms can be distinguished by some factors, such as temperature and viscosity. For dynamic quenching, higher temperatures increase diffusion coefficients due to decreased viscosity and the bimolecular quenching constants increase with increasing temperature. However, for static quenching, an increase in temperature leads to a decrease of stability of complexes formed between the fluorophore/quencher, and thus decreases the values of the Stern-Volmer constant with increasing temperatures [49].

The quenching mechanism involved can be examined using the Stern-Volmer Eq. (1):

$$F_0/F = 1 + k_q\tau_0[Q] = 1 + K_{sv}[Q] \quad (1)$$

where, F_0 and F are the fluorescence of HSA in the absence and presence of ruthenium complexes, K_{sv} is the Stern-Volmer constant, [Q] is the concentration of ruthenium complexes, k_q is the bimolecular quenching constant and τ_0 is the average lifetime of the fluorophore in the absence of quencher [51].

The K_{sv} constant decrease when the temperature is increased from 298 to 310 K (Table 2), indicating a static mechanism of quenching. In addition, evidence of the static mechanism is the k_q values of the order of 10^{11} and $10^{12}\,Ms^{-1}$ (Table 2). These values are greater than the maximum value possible for dynamic quenching ($2 \times 10^{10}\,LMs^{-1}$.

The fluorescence quenching data were analyzed to obtain the binding constant (K_b) and number of binding sites (*n*) using Eq. (2):

$$\log\frac{(F_0 - F)}{F} = \log K_b + n\log[Q] \quad (2)$$

The K_b and *n* can be calculated by plotting $\log[(F_0 - F)/F]$ versus $\log[Q]$, as shown in Fig. 3(C). The K_b values confirm a higher interaction between the ruthenium complexes and HSA comparatively to other ruthenium complexes reported in the literature [52]. The values of the n indicate that ruthenium complexes interact by only one binding site.

To evaluate the types of interactions that occur between the complexes and the HSA, some thermodynamic parameters were obtained. The thermodynamic parameters as free energy (ΔG°), enthalpy (ΔH°) and entropy (ΔS°) were calculated using Eqs. (3) and (4):

$$\ln\left(\frac{K_{b1}}{K_{b2}}\right) = \left(\frac{1}{T_1} - \frac{1}{T_2}\right) \times \frac{\Delta H^\circ}{R} \quad (3)$$

$$\Delta G^\circ = -RT\ln K_b = \Delta H^\circ - T\Delta S^\circ \quad (4)$$

where K_{b1} and K_{b2} are the binding constants in temperature T_1 and T_2 and R is the gas constant [52].

Table 3 shows the thermodynamic parameters for ruthenium complexes and HSA. The thermodynamic parameters, enthalpy change (ΔH), entropy change (ΔS) and free energy change (ΔG), are the main means used to confirm the binding modes. From the thermodynamic standpoint, $\Delta H > 0$ and $\Delta S > 0$ imply a hydrophobic interaction; $\Delta H < 0$ and $\Delta S < 0$ reflects van der Waals force or hydrogen bond formation; and $\Delta H < 0$ and $\Delta S > 0$ suggests an electrostatic force. Thus, the negatives values for ΔH°, ΔS° and ΔG° indicates the van der Waals force or hydrogen bonding formation and the spontaneous interaction between protein and the complexes [53].

3.4. Biological activity

3.4.1. MTT assay

In order to evaluate the cytotoxic activity of the ruthenium complexes upon coordination of lawsone compared with free ligand, the in vitro assays were carried out against prostate (DU-145), breast (MCF-7) and the lung (A549) tumor cell line and compared with the lung non-tumor cell line (MRC-5). Cisplatin was used for comparison, under identical conditions. In this assay, the compounds were incubated with cells for 48 h. As can be seen by the results summarized in Table 4, the ruthenium complexes were more active than cisplatin and the free ligand lawsone for all cells evaluated. All the complexes were very active against the tumor cells, mainly complex (**5**), reaching nanomolar concentrations, especially on the A549 cell line. Importantly, complex (**5**) is less toxic against lung non-tumor cells, suggesting selectivity for lung

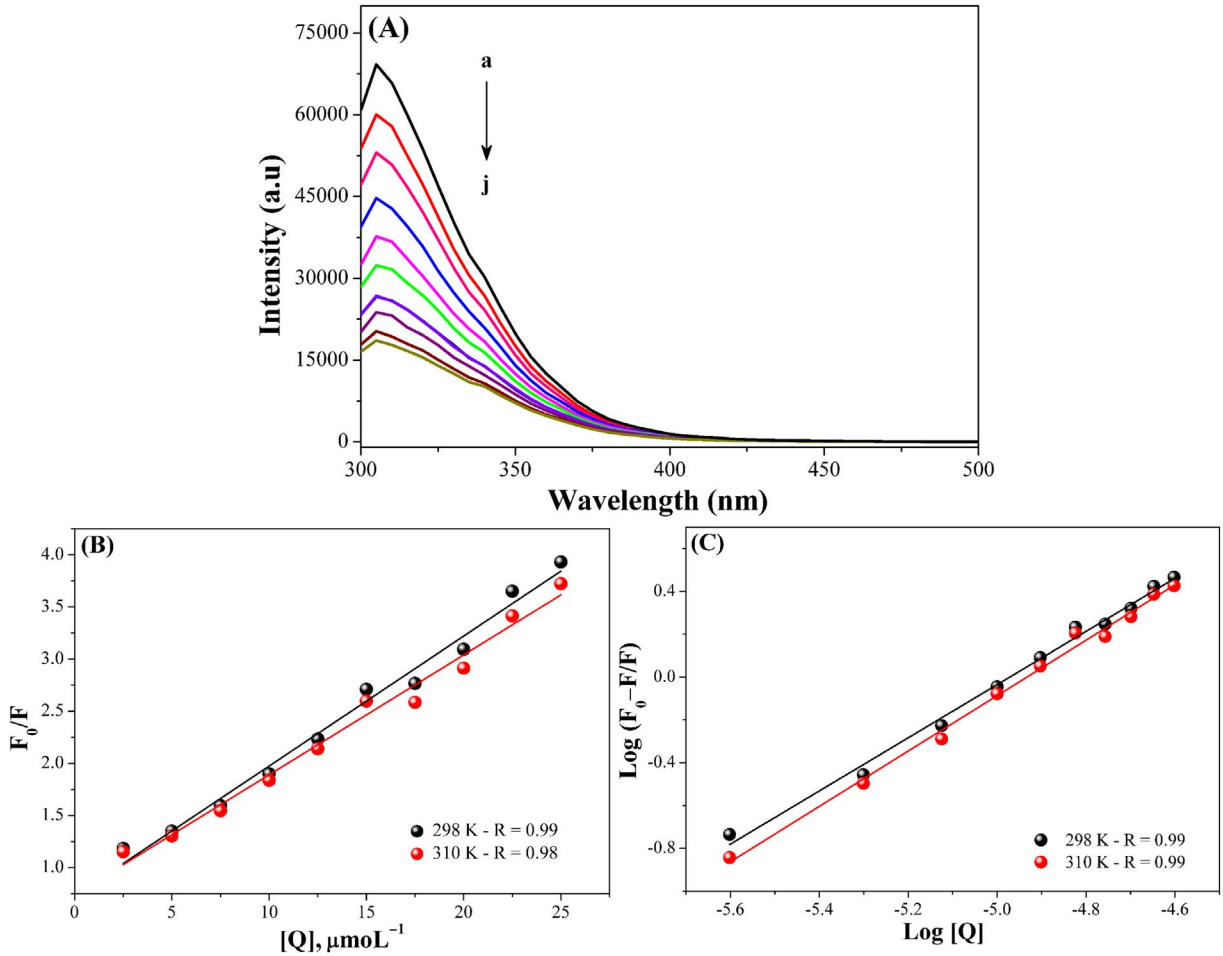

Fig. 3. (A) Fluorescence spectra of HSA (5 μM) with increasing concentrations of complex (**5**). (B) Stern-Volmer plots for the quenching of HSA in the presence of complex (**5**). (C) Plot of log[(F_0 − F) / F] vs. log[Q].

Table 2
Quenching parameters for the interactions of ruthenium complexes (**1**–**5**) with HSA.

Complexes	K_{sv} (M^{-1})	k_q ($M^{-1}\,s^{-1}$)	K_b (M^{-1})	*n*
(**1**)	(9.97 ± 0.08) × 10^4	9.97 × 10^{11}	(2.13 ± 0.22) × 10^5	1.09
	(8.47 ± 0.13) × 10^4	8.47 × 10^{11}	(1.38 ± 0.71) × 10^5	0.98
(**2**)	(9.32 ± 0.20) × 10^4	9.32 × 10^{11}	(2.45 ± 0.12) × 10^6	1.23
	(7.59 ± 0.03) × 10^4	7.59 × 10^{11}	(1.50 ± 0.42) × 10^6	1.52
(**3**)	(1.15 ± 0.02) × 10^4	1.15 × 10^{11}	(2.03 ± 0.31) × 10^6	1.28
	(1.10 ± 0.09) × 10^4	1.10 × 10^{11}	(1.38 ± 0.24) × 10^6	1.55
(**4**)	(1.14 ± 0.06) × 10^5	1.14 × 10^{12}	(2.15 ± 0.60) × 10^6	1.22
	(1.03 ± 0.02) × 10^5	1.03 × 10^{12}	(1.50 ± 0.29) × 10^6	1.28
(**5**)	(1.24 ± 0.02) × 10^5	1.24 × 10^{12}	(2.60 ± 0.16) × 10^6	1.22
	(1.15 ± 0.03) × 10^5	1.15 × 10^{12}	(1.87 ± 0.15) × 10^6	1.28

Table 3
Thermodynamic parameters for interaction between complexes (**1**–**5**) and HSA.

Complexes	ΔG° (kJ mol^{-1})	ΔH° (kJ mol^{-1})	ΔS° (J $mol^{-1}\,K^{-1}$)
(**1**)	− 30.40	− 27.76	− 8.86
(**2**)	− 36.45	− 31.38	− 17.01
(**3**)	− 35.98	− 24.70	− 37.85
(**4**)	− 36.12	− 23.04	− 43.89
(**5**)	− 36.60	− 21.09	− 52.05

cancer cells. Probably, the presence of the 4,7-diphenyl-1,10-phenanthroline (phphen) ligand in the complex (**5**) can contribute to increasing antitumor activity, as previously observed for other ruthenium complexes, where the increase of the phenyl ring substituents on the *N*,*N*-chelating ligand, is directly related to the increase of biological activity [54]. Therefore, complex (**5**) was selected for detailed studies of mechanism of cell death.

The morphological changes caused by different concentrations of complex (**5**) on A549 and MRC-5 cell lines were registered using an inverted microscopic coupled to a camera, after 24 and 48 h of incubation. Remarkable changes were observed on cell morphology after 48 h of incubation at concentrations of 0.1, 2, 5 and 10 μM for A549 cells and 2, 5 and 10 μM for MRC-5 cells, when compared with the controls (Fig. 4). The appearance of the circular structures, loss of cell adhesion, cell contraction and the formation of cell aggregates was observed, all indicating cell death. These observations are consistent with results from the MTT assay, indicating that complex (**5**) suppresses cell growth and proliferation, presenting higher selectivity against lung

Table 4
The cytotoxicity activity for ruthenium complexes (**1–5**) in human cell lines.

Compounds	IC_{50} (μM)				
	DU-145	MCF-7	A549	MRC-5	SI[a]
Law	> 100	> 100	> 100	> 100	–
(**1**)	0.15 ± 0.03	0.41 ± 0.04	0.20 ± 0.06	0.98 ± 0.12	4.9
(**2**)	1.28 ± 0.33	0.45 ± 0.02	0.21 ± 0.01	0.54 ± 0.07	2.6
(**3**)	0.16 ± 0.01	0.26 ± 0.02	0.24 ± 0.03	1.34 ± 0.27	5.6
(**4**)	1.93 ± 0.57	0.31 ± 0.03	0.13 ± 0.01	0.56 ± 0.05	4.3
(**5**)	0.77 ± 0.06	0.13 ± 0.02	0.09 ± 0.01	1.44 ± 0.25	16.0
Cisplatin	2.33 ± 0.40	13.98 ± 2.02	14.42 ± 1.45	29.09 ± 0.78	2.0

[a] SI = Selectivity index for lung cells = IC_{50} of MRC-5/IC_{50} of A549.

cancer, when compared to other cell lines.

3.4.2. Migration assays

Subsequently, the cell migration assays were performed to evaluate the anti-metastatic capability of the complex (**5**). It is well known that metastasis is a biological process in carcinomas that relies on cell migration and invasion to other regions of the body [55,56]. Therefore, in this study, we evaluated the anti-migratory properties of complex (**5**).

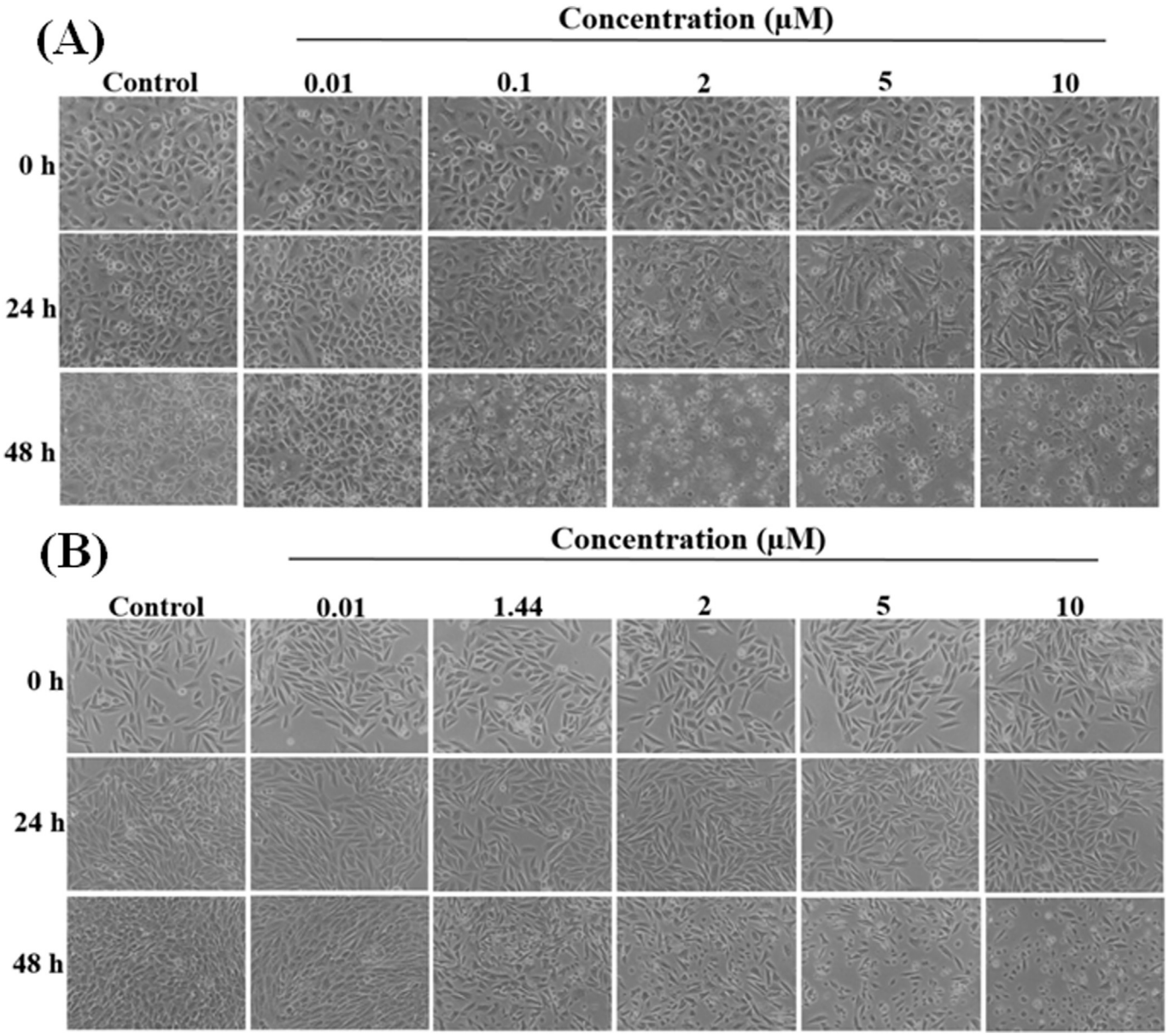

Fig. 4. Cellular morphology of A549 (A) and MRC-5 (B) treated with complex (**5**) for 24 and 48 h. Cell morphology was examined under an inverted microscope and acquired using a 10 × objective.

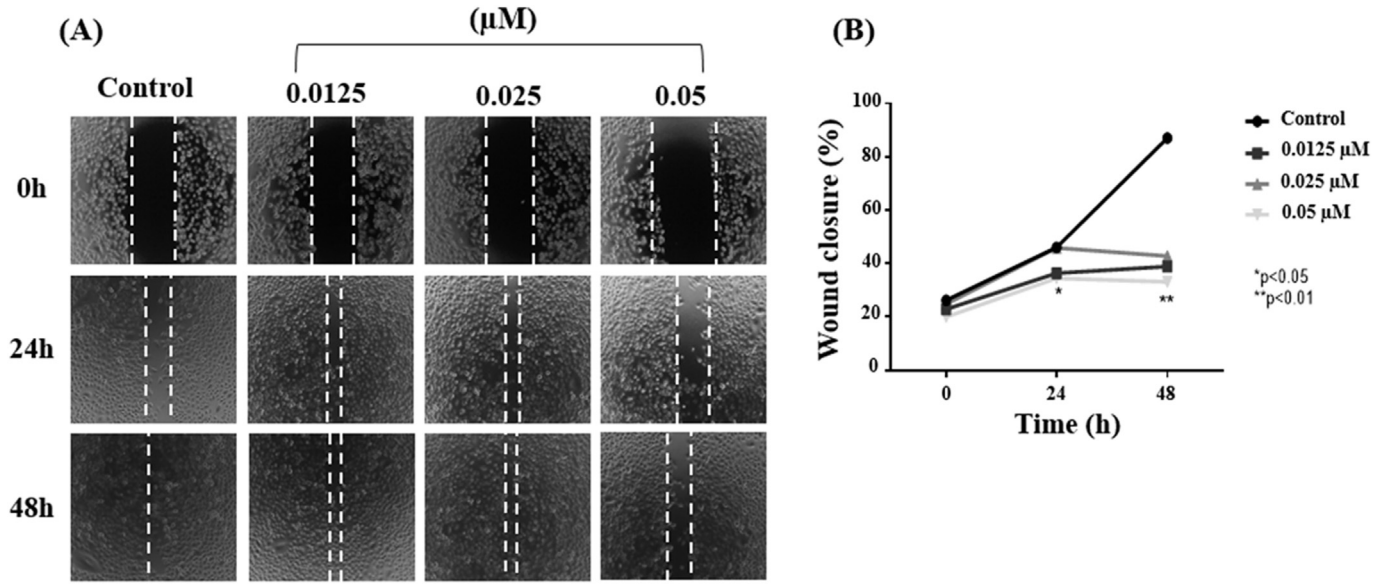

Fig. 5. Wound-healing assay showing complex (**5**). (A) The images show the effects of complex (**5**) on the migration of the A549 cell line. (B) Results from measurements of the area of the scratch. The data are presented as mean ± SD (n = 3).

The anti-migratory properties were examined using the wound-healing scratch and transwell migration assays. For wound healing assay, the cells were treated with different concentrations of ruthenium complex (**5**). Concentrations below the IC_{50} value (0.09 ± 0.01 μM, in 48 h) were chosen to be used in this assay. The images were registered at different time points after the treatment. As can be seen in Fig. 5, the treatment of the cells with complex (**5**) leads to the inhibition of their migration, mainly at a concentration of 0.05 μM where an inhibition of 70% of wound closure was observed.

As can be observed in Fig. 6, the cells migrated to the chamber containing fetal bovine serum and free of complex (**5**) (Control +, FBS +). On the other hand, in the chamber containing only culture medium, free of both fetal bovine serum and complex (**5**), there was no cell migration (Control −, FBS −). Results were similar using the Boyden chamber assay. Complex (**5**) at 0.05, 0.025 and 0.0125 μM inhibited the migration of A549 cells by 85, 65 and 47%, respectively. These results indicate that complex (**5**) is a potent inhibitor of A549 cell migration.

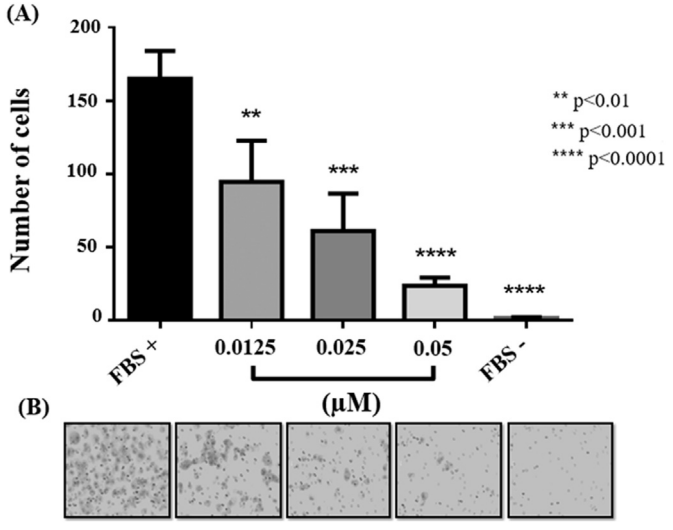

Fig. 6. Effects of complex (**5**) on the A549 migration. (A) Quantitative analysis of the cell migration by Image J software. (B) Representative images (10 ×) showed the cells that migrated on the surface of the filter. The bars represent mean ± SD from three independent experiments.

3.4.3. Cell cycle assay

Studies in cell lines led to the proposal of mechanism on the action of the potential drugs, and some ruthenium complexes have demonstrated the ability to inhibit cancer cell growth by arresting their cycle [57,58]. In order to evaluate the influence of complex (**5**) in the cell cycle, A549 tumor cells were treated with different concentrations of complex (**5**) for 24 h. The cell cycle was analyzed via the PI (Propidium Iodide) staining and flow cytometry. As shown in Fig. 7, the cell distribution analysis obtained demonstrates clear enhancement of the cell number at sub G1 (24.65 ± 0.35, 32.85 ± 1.35, 48.2 ± 4.1 and 52.7 ± 3.0% for control, 1, 2 and 3 μM, respectively). In addition, the number of cells at the S phase decreased, in a concentration-dependent manner (7.95 ± 0.25, 13.4 ± 0.6, 7.0 ± 0.1 and 3.55 ± 0.35% for control, 1, 2 and 3 μM, respectively). Based on these results, we suggest that the antiproliferative effects of complex (**5**) on A549 cells occur by apoptosis, as reflected by the arrest at the sub G1 phase.

3.4.4. Cell apoptosis assay by PE Annexin V

Apoptosis is characterized by programmed cell death and controls the development and homeostasis in multicellular organisms. The

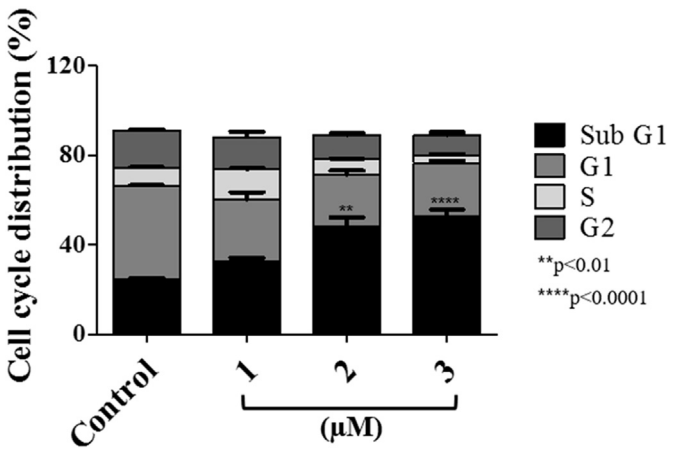

Fig. 7. Quantitative cell cycle distribution for A549 cells after treatment with complex (**5**) for 24 h. Data are expressed as mean ± SD of three independent measurements.

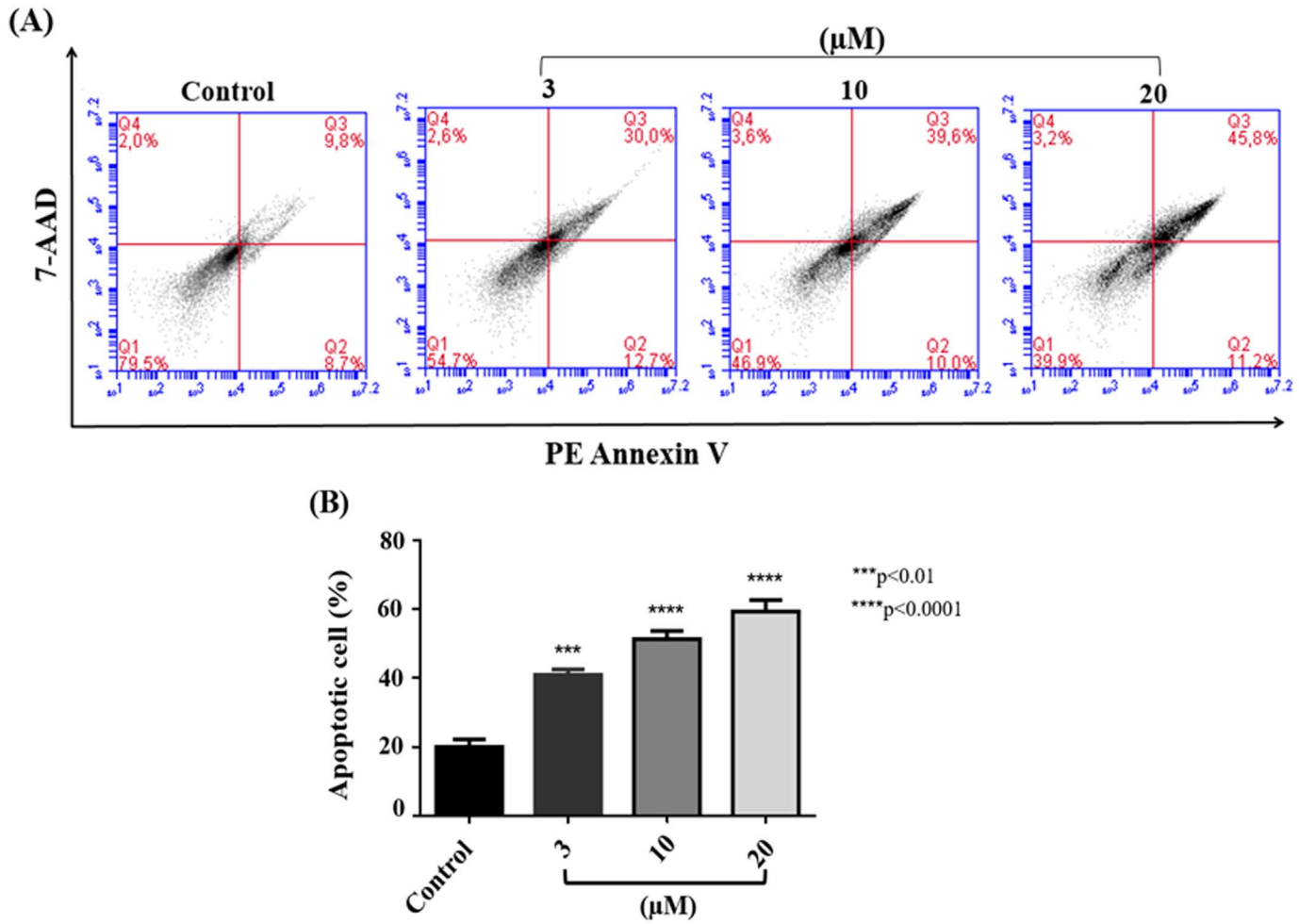

Fig. 8. Induction of apoptosis. (A) Flow cytometric analysis of apoptosis using PE Annexin V-7AAD double staining of A549 cells treated with different concentrations of complex (**5**) for 24 h. Data are representative of one of two individual experiments. (B) Graph of the proportion of cells in apoptosis (early + late stages) for different concentrations of complex (**5**) in comparison with the control.

contribution of apoptosis to cancer has been extensively investigated since many anticancer drugs exhibit their effects by inducing apoptosis [59,60]. The ability of complex (**5**) to promote cell death by apoptosis or necrosis was investigated by flow cytometry after staining the cells with PE Annexin V with 7-AAD. Fig. 8 shows the results of the flow cytometric analysis. The PE Annexin V-7AAD plots are divided into four quadrants in order to distinguish each cell stage. The cells, which were not viable, did not bind to PE Annexin V or 7AAD and were arranged in the lower left quadrant. Cells in early apoptotic stages are PE Annexin V positive and 7-AAD negative (lower right quadrant), resulting in green fluorescence. Cells in late apoptosis stages are both PE Annexin V and 7-AAD positive (upper right quadrant) resulting in a strong green and red fluorescence. The upper left quadrant corresponds to necrotic cells. The incubation of A549 cells with increasing concentrations of complex (**5**) produced a considerable increase in the percentage of apoptotic cells (Q2 and Q3 quadrants). In the control, the percentage of apoptotic cells was 18.5% (early + late stages). After the treatment with complex (**5**) at 3, 10 and 20 μM, the percentages of apoptotic cells (early + late stages) increased to 42.7, 49.6 and 57%, respectively. These results show that complex (**5**) induces cell death by apoptosis.

4. Conclusions

In summary, five new ruthenium complexes were synthesized, characterized and investigated for their ability to interact with CT-DNA and HSA and whether they cause cytotoxic effects in different tumor cell lines. Complex/DNA interaction studies have demonstrated a weak capacity of these complexes to distort the DNA secondary structure. Thus, the DNA cannot be the primordial target for these complexes, and the antitumor activity may be related to others protein targets (e.g., topoisomerase, kinase). On the other hand, complex/protein interaction studies have shown the capability of these complexes to bind to HSA, indicating that the ruthenium complexes can be distributed and transported in the body by HSA, ensuring their biological activity.

All complexes (**1–5**) showed remarkable cytotoxicity against the MCF-7 (breast), DU-145 (prostate) and A549 (lung) tumor cell lines, and considerably less cytotoxicity to MRC-5 (lung) non-tumor cells. In addition, the complexes were more cytotoxic compared to the free ligand lawsone and the widely used anticancer drug cisplatin, under identical conditions.

Complex (**5**) showed growth inhibition against all cell lines tested, presenting high selectivity, especially, on the lung A549 cell line with IC_{50} value at nanomolar level. The investigation of the mechanism of cell death showed that complex (**5**) is a potent inhibitor of cell migration and producing death of A549 tumor cells through an apoptotic pathway. Moreover, cell cycle analysis shows that complex (**5**) can induce A549 cell cycle arrest at the Sub G1 phase. Therefore, the work reported here showed promising antitumor candidates that can be further studied as a potent chemotherapeutic agent for human tumor treatment.

Acknowledgements

We would like to thank the Brazilian Agencies of Research: CAPES, CNPq and FAPESP. We thank Murilo Carrocia by the contribution with crystal structure determination. K. M. Oliveira would like to thank FAPESP for a research fellowship (grant number 2014/04147-9). R. S. Correa would also like to thank CNPq for the financial support (project 403588/2016-2).

Appendix A. Supplementary data

Supplementary data to this article can be found online at http://dx.doi.org/10.1016/j.jinorgbio.2017.08.019.

References

[1] L. Kelland, Nat. Rev. Cancer 7 (2007) 573–584.
[2] N.P. Farrell, Semin. Oncol. 14 (2004) 1–9.
[3] J. Fernandez-Gallardo, B.T. Elie, T. Sadhukha, S. Prabha, M. Sanau, S.A. Rotenberg, J.W. Ramos, M. Contel, Chem. Sci. 6 (2015) 5269–5283.
[4] M. Kubanik, W. Kandioller, K. Kim, R.F. Anderson, E. Klapproth, M.A. Jakupec, A. Roller, T. Sohnel, B.K. Keppler, C.G. Hartinger, Dalton Trans. 45 (2016) 13091–13103.
[5] C.A. Rabik, M.E. Dolan, Cancer Treat. Rev. 33 (2007) 9–23.
[6] Z. Liu, A. Habtemariam, A.M. Pizarro, S.A. Fletcher, A. Kisova, O. Vrana, L. Salassa, P.C.A. Bruijnincx, G.J. Clarkson, V. Brabec, P.J. Sadler, J. Med. Chem. 54 (2011) 3011–3026.
[7] S.H. van Rijt, I. Romero-Canelon, Y. Fu, S.D. Shnyder, P.J. Sadler, Metallomics 6 (2014) 1014–1022.
[8] I. Romero-Canelón, P.J. Sadler, Inorg. Chem. 52 (2013) 12276–12291.
[9] G. Sava, G. Jaouen, E.A. Hillard, A. Bergamo, Dalton Trans. 41 (2012) 8226–8234.
[10] A. Bergamo, G. Sava, Dalton Trans. (2007) 1267–1272.
[11] B.S. Murray, M.V. Babak, C.G. Hartinger, P.J. Dyson, Coord. Chem. Rev. 306 (2016) 86–114.
[12] R. Trondl, P. Heffeter, C.R. Kowol, M.A. Jakupec, W. Berger, B.K. Keppler, Chem. Sci. 5 (2014) 2925–2932.
[13] M.V. Babak, S.M. Meier, K.V.M. Huber, J. Reynisson, A.A. Legin, M.A. Jakupec, A. Roller, A. Stukalov, M. Gridling, K.L. Bennett, J. Colinge, W. Berger, P.J. Dyson, G. Superti-Furga, B.K. Keppler, C.G. Hartinger, Chem. Sci. 6 (2015) 2449–2456.
[14] J. Kljun, A.K. Bytzek, W. Kandioller, C. Bartel, M.A. Jakupec, C.G. Hartinger, B.K. Keppler, I. Turel, Organometallics 30 (2011) 2506–2512.
[15] S. Chatterjee, S. Kundu, A. Bhattacharyya, C.G. Hartinger, P.J. Dyson, J. Biol. Inorg. Chem. 13 (2008) 1149–1155.
[16] P. Mehlen, A. Puisieux, Nat. Rev. Cancer 6 (2006) 449–458.
[17] K.W. Wellington, RSC Adv. 5 (2015) 20309–20338.
[18] V.K. Tandon, S. Kumar, Expert Opin. Ther. Pat. 23 (2013) 1087–1108.
[19] M.R.S. Kumar, K. Aithal, B.N. Rao, N. Udupa, B.S.S. Rao, Toxicol. in Vitro 23 (2009) 242–250.
[20] S.-T. Huang, H.-S. Kuo, C.-L. Hsiao, Y.-L. Lin, Bioorg. Med. Chem. 10 (2002) 1947–1952.
[21] M.I.F. Barbosa, R.S. Corrêa, K.M. de Oliveira, C. Rodrigues, J. Ellena, O.R. Nascimento, V.P.C. Rocha, F.R. Nonato, T.S. Macedo, J.M. Barbosa-Filho, M.B.P. Soares, A.A. Batista, J. Inorg. Biochem. 136 (2014) 33–39.
[22] U.A. Dar, S. Bhand, D.N. Lande, S.S. Rao, Y.P. Patil, S.P. Gejji, M. Nethaji, T. Weyhermüller, S. Salunke-Gawali, Polyhedron 113 (2016) 61–72.
[23] I. Casanova, A. Sousa-Pedrares, J. Viqueira, M.L. Duran, J. Romero, A. Sousa, J.A. Garcia-Vazquez, New J. Chem. 37 (2013) 2303–2316.
[24] F.L. Bustamante, J.M. Metello, F.A. de Castro, C.B. Pinheiro, M.D. Pereira, M. Lanznaster, Inorg. Chem. 52 (2013) 1167–1169.
[25] M.A. Ribeiro, M. Lanznaster, M.M. Silva, J.A. Resende, M.V. Pinheiro, K. Krambrock, H.O. Stumpf, C.B. Pinheiro, Dalton Trans. 42 (2013) 5462–5470.
[26] W. Kandioller, E. Balsano, S.M. Meier, U. Jungwirth, S. Goschl, A. Roller, M.A. Jakupec, W. Berger, B.K. Keppler, C.G. Hartinger, Chem. Commun. 49 (2013) 3348–3350.
[27] R.S. Corrêa, M.M. da Silva, A.E. Graminha, C.S. Meira, J.A.F.d. Santos, D.R.M. Moreira, M.B.P. Soares, G. Von Poelhsitz, E.E. Castellano, C. Bloch Jr., M.R. Cominetti, A.A. Batista, J. Inorg. Biochem. 156 (2016) 153–163.
[28] R.S. Correa, K.M. de Oliveira, F.G. Delolo, A. Alvarez, R. Mocelo, A.M. Plutin, M.R. Cominetti, E.E. Castellano, A.A. Batista, J. Inorg. Biochem. 150 (2015) 63–71.
[29] L. Colina-Vegas, W. Villarreal, M. Navarro, C.R. de Oliveira, A.E. Graminha, P.I.d.S. Maia, V.M. Deflon, A.G. Ferreira, M.R. Cominetti, A.A. Batista, J. Inorg. Biochem. 153 (2015) 150–161.
[30] L. Colina-Vegas, J.L. Dutra, W. Villarreal, J.H. de A.N., M.R. Cominetti, F. Pavan, M. Navarro, A.A. Batista, J. Inorg. Biochem. 162 (2016) 135–145.
[31] A.A. Batista, M.O. Santiago, C.L. Donnici, I.S. Moreira, P.C. Healy, S.J. Berners-Price, S.L. Queiroz, Polyhedron 20 (2001) 2123–2128.
[32] G. Sheldrick, Acta Crystallogr. C 71 (2015) 3–8.
[33] T. Chatterjee, A. Pal, S. Dey, B.K. Chatterjee, P. Chakrabarti, PLoS One 7 (2012) e37468.
[34] A.M. El-Hendawy, Polyhedron 10 (1991) 2511–2518.
[35] S. Salunke-Gawali, L. Kathawate, V.G. Puranik, J. Mol. Struct. 1022 (2012) 189–196.
[36] G. Valle-Bourrouet, V.M. Ugalde-Saldívar, M. Gómez, L.A. Ortiz-Frade, I. González, C. Frontana, Electrochim. Acta 55 (2010) 9042–9050.
[37] F.L.S. Bustamante, M.M.P. Silva, W.A. Alves, C.B. Pinheiro, J.A.L.C. Resende, M. Lanznaster, Polyhedron 42 (2012) 43–49.
[38] K. Nakamoto, Fourth ed. Wiley ed., New York (2009).
[39] R.A. Farfán, J.A. Espíndola, M.A. Martínez, O.E. Piro, P.J. Aymonino, J. Coord. Chem. 62 (2009) 3738–3744.
[40] I. Singh, R.T. Ogata, R.E. Moore, C.W.J. Chang, P.J. Scheuer, Tetrahedron 24 (1968) 6053–6073.
[41] O.M. Santiago, A.A. Batista, P.M. de Araújo, L.C. Donnici, d.S.I. Moreira, E.E. Castellano, J. Ellena, d.S. Santos, S.L. Queiroz, Transit. Met. Chem. 30 (2005) 170–175.
[42] K.M. Oliveira, R.S. Corrêa, M.I.F. Barbosa, J. Ellena, M.R. Cominetti, A.A. Batista, Polyhedron 130 (2017) 108–114.
[43] A.V. Todkary, R. Dalvi, S. Salunke-Gawali, J. Linares, F. Varret, J. Marrot, J.V. Yakhmi, M. Bhadbhade, D. Srinivas, S.P. Gejji, S.Y. Rane, Spectrochim. Acta A 63 (2006) 130–138.
[44] M. Frik, J. Fernandez-Gallardo, O. Gonzalo, V. Mangas-Sanjuan, M. Gonzalez-Alvarez, A. Serrano del Valle, C. Hu, I. Gonzalez-Alvarez, M. Bermejo, I. Marzo, M. Contel, J. Med. Chem. 58 (2015) 5825–5841.
[45] L. Li, Q. Guo, J. Dong, T. Xu, J. Li, J. Photochem. Photobiol. B 125 (2013) 56–62.
[46] V.M. Manikandamathavan, T. Weyhermuller, R.P. Parameswari, M. Sathishkumar, V. Subramanian, B.U. Nair, Dalton Trans. 43 (2014) 13018–13031.
[47] M. Frik, A. Martínez, B.T. Elie, O. Gonzalo, D.R. Mingo, M. Sanaú, R. Sánchez-Delgado, T. Sadhukha, S. Prabha, J.W. Ramos, I. Marzo, M.J. Contel, Med. Chem. 57 (2014) 9995–10012.
[48] L. Corte-Real, F. Mendes, J. Coimbra, T.S. Morais, A.I. Tomaz, A. Valente, M.H. Garcia, I. Santos, M. Bicho, F.J. Marques, J. Biol. Inorg. Chem. 19 (2014) 853–867.
[49] T.S. Morais, F.C. Santos, T.F. Jorge, L. Côrte-Real, P.J.A. Madeira, F. Marques, M.P. Robalo, A. Matos, I. Santos, M.H. Garcia, J. Inorg. Biochem. 130 (2014) 1–14.
[50] F. Xue, C.-Z. Xie, Y.-W. Zhang, Z. Qiao, X. Qiao, J.-Y. Xu, S.-P. Yan, J. Inorg. Biochem. 115 (2012) 78–86.
[51] J.R. Lakowicz, Principles of Fluorescence Spectroscopy, Third ed., Springer, New York, 2009.
[52] M. Ganeshpandian, R. Loganathan, E. Suresh, A. Riyasdeen, M.A. Akbarsha, M. Palaniandavar, Dalton Trans. 43 (2014) 1203–1219.
[53] P.D. Ross, S. Subramanian, Biochemistry 20 (1981) 3096–3102.
[54] R. Carter, A. Westhorpe, M.J. Romero, A. Habtemariam, C.R. Gallevo, Y. Bark, N. Menezes, P.J. Sadler, R.A. Sharma, Sci Rep 6 (2016) 20596.
[55] H. Yamaguchi, J. Wyckoff, J. Condeelis, Curr. Opin. Cell Biol. 17 (2005) 559–564.
[56] A. Valster, N.L. Tran, M. Nakada, M.E. Berens, A.Y. Chan, M. Symons, Methods 37 (2005) 208–215.
[57] L.-m. Chen, F. Peng, G.-d. Li, X.-m. Jie, K.-r. Cai, C. Cai, Y. Zhong, H. Zeng, W. Li, Z. Zhang, J.-c. Chen, J. Inorg. Biochem. 156 (2016) 64–74.
[58] Z. Zhao, Z. Luo, Q. Wu, W. Zheng, Y. Feng, T. Chen, Dalton Trans. 43 (2014) 17017–17028.
[59] R.S. Wong, J. Exp. Clin. Cancer Res. 30 (2011) 87.
[60] C.P. Tan, Y.Y. Lu, L.N. Ji, Z.W. Mao, Metallomics 6 (2014) 978–995.